Acta Mech Sin (2006) 22:547–557
DOI 10.1007/s10409-006-0039-0

RESEARCH PAPER

Seismic responses of a hemispherical alluvial valley to SV waves: a three-dimensional analytical approximation

Chenggang Zhao · Jun Dong · Fuping Gao · D.-S. Jeng

Received: 4 January 2006 / Revised: 21 July 2006 / Accepted: 21 July 2006 / Published online: 16 November 2006

Abstract An analytical solution to the three-dimensional scattering and diffraction of plane SV-waves by a saturated hemispherical alluvial valley in elastic half-space is obtained by using *Fourier–Bessel* series expansion technique. The hemispherical alluvial valley with saturated soil deposits is simulated with Biot's dynamic theory for saturated porous media. The following conclusions based on numerical results can be drawn: (1) there are a significant differences in the seismic response simulation between the previous single-phase models and the present two-phase model; (2) the normalized displacements on the free surface of the alluvial valley depend mainly on the incident wave angles, the dimensionless frequency of the incident SV waves and the porosity of sediments; (3) with the increase of the incident angle, the displacement distributions become more complicated; and the displacements on the free surface of the alluvial valley increase as the porosity of sediments increases.

Keywords Biot's dynamic theory · Saturated porous media · Three-dimensional scattering · Hemispherical alluvial valley

1 Introduction

In the recent three decades, the seismic responses of a local irregular site have drawn much attention of geotechnical engineers, seismologists and earthquake engineers. It has been observed that the sediment conditions of a local site have significant effects upon amplification of ground motions during earthquakes. One of the examples is the Michoacon, Mexico, earthquake in 1985 [1]. As reported in [1], two strong shocks caused a middle level destruction in the areas near the epicenter, but more severe damages in the Mexico City, which is far from the epicenter and located on a thick bathtub soft clay stratification. It was reported that the earthquake-induced ground motion of basin is magnified six times or even more, and the aggregation and magnification of seismic waves in the basin is the main reason for the serious damages. Similar phenomena were also observed during the Lima, Peru, earthquake [2]. Till now, the motion magnification of an irregular alluvial valley during an earthquake has not been well simulated and understood.

Since Trifunac [3] proposed a two-dimensional analytical solution to the scattering of plane SH waves by a semi-circular canyon, numerous two-dimensional approaches have been proposed for the analysis of the effects of surface topography and geological conditions

The project was supported by the National Natural Science Foundation of China (50478062 and 10532070) and Open Fund at the Key Laboratory of Urban Security and Disaster Engineering (Beijing University of Technology), Chinese Ministry of Education. The English text was polished by Keren Wang.

C. Zhao · J. Dong
School of Civil Engineering and Architecture,
Beijing Jiaotong University,
Beijing 100044, China

F. Gao (✉)
Institute of Mechanics, Chinese Academy of Sciences,
Beijing 100080, China
e-mail: fpgao@imech.ac.cn

D.-S. Jeng
School of Civil Engineering, The University of Sydney,
Sydney, NSW 2006, Australia

on elastic wave propagation [3–8]. A few attempts have also been made to investigate the three-dimensional cases [9–13]. Among these, Lee [11,12] developed an analytical solution to the three-dimensional scattering and diffraction of plane waves by hemispherical canyons and hemispherical alluvial valleys, using Fourier–Bessel series expansion technique.

All aforementioned analytical solutions are for seismic waves propagating in a single-phase elastic medium. In reality, the irregular soft clay deposit would be more reasonably simulated as a two-phase porous medium than as a single-phase medium. To date, only a few two-dimensional models [14,15] have been developed to investigate the scattering and diffraction of plane waves by a saturated circular cylindrical canyon, and these two-dimensional models do not adequately represent the realistic conditions of a hemispherical alluvial valley. Thus, a three-dimensional model is desirable for the scattering and diffraction of plane waves by a hemispherical alluvial valley.

In this paper, an analytic solution to the three-dimensional scattering and diffraction of plane SV waves by a hemispherical alluvial valley is derived. The Biot's dynamic theory for saturated porous media [16] is employed to simulate soft clay deposit in the hemispherical alluvial valley, and the half space is considered as a single-phase elastic medium. A comprehensive comparison is made between the present two-phase model and the previous single-phase model, and a parametric study is conducted to examine the influences of the local site condition on the amplification of earthquake-induced surface displacements.

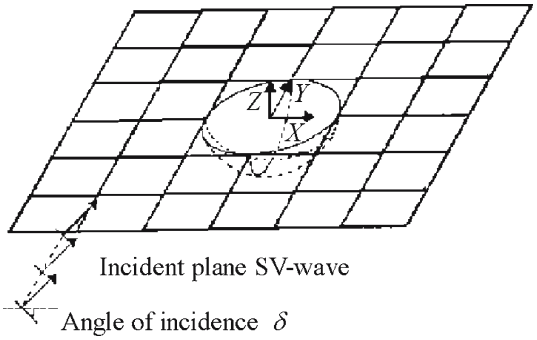

Fig. 1 A half-space with a hemisphere alluvial valley and an incident SV wave

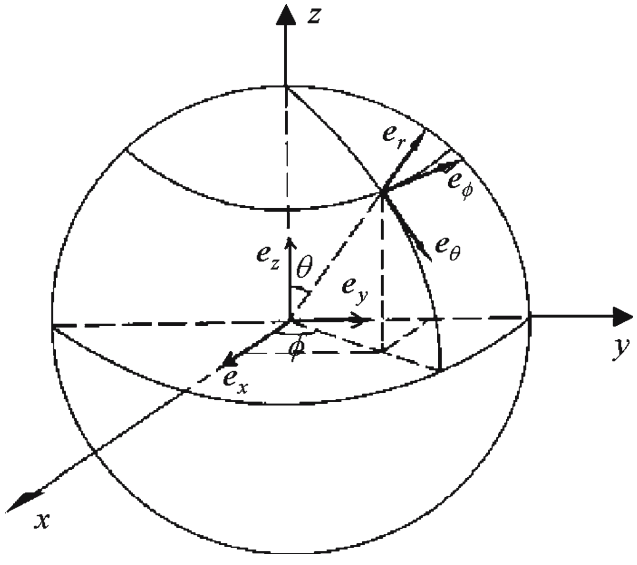

Fig. 2 Spherical and rectangular coordinates

2 Theoretical formulations

2.1 Boundary value problem

We consider a three-dimensional problem of scattering and diffraction of SV waves with incident angle δ by a soft saturated hemispherical alluvial valley with a radius $r = a$ inlaying the half-space, as depicted in Fig. 1. The half-space is assumed to be a single-phase elastic homogeneous and isotropic medium, while the hemispherical alluvial valley is a two-phase homogeneous saturated porous medium. Note that the hemispherical alluvial valley was considered as a one-phase elastic medium in previous investigations [11,12]. The geometry of the model is described with spherical coordinates (r, θ, ϕ), as shown in Fig. 2. The rectangular coordinate system is employed simultaneously and the relation between the two coordinate systems is shown in Fig. 2.

Given a function $F(r,\theta,\phi,t)$ of space and time, the wave equation in spherical coordinates is written as

$$\frac{1}{r^2}\frac{\partial}{\partial r}\left(r^2\frac{\partial F}{\partial r}\right)+\frac{1}{r^2\sin\theta}\frac{\partial}{\partial\theta}\left(\sin\theta\frac{\partial F}{\partial\theta}\right)+\frac{1}{r^2\sin^2\theta}\frac{\partial^2}{\partial\phi^2}-\frac{1}{c^2}\frac{\partial^2 F}{\partial t^2}=0, \tag{1}$$

in which c is the wave velocity. After separation of variables, a general harmonic solution of Eq. (1) can be expressed as

$$Z_n^{(j)}(kr)P_n^m(\mu)\begin{matrix}\cos\\ \sin\end{matrix}m\phi\exp(-\mathrm{i}\omega t), \tag{2}$$

in which $m,n = 0,1,2,\ldots$, and $m \le n$; k is the wave number, $k = \omega/c$, in which ω is the harmonic frequency; $P_n^m(\mu)$ is an associated Legendre polynomial with $\mu = \cos\theta$; $Z_n^{(j)}(j = 1,2,3,4)$ denote the spherical Bessel and Hankel functions as follows:

$$Z_n^{(1)}(kr) \equiv \mathrm{j}_n(kr) = \left(\frac{\pi}{2kr}\right)^{1/2} \mathrm{J}_{n+1/2}(kr), \tag{3a}$$

$$Z_n^{(2)}(kr) \equiv \mathrm{y}_n(kr) = \left(\frac{\pi}{2kr}\right)^{1/2} \mathrm{Y}_{n+1/2}(kr), \tag{3b}$$

$$Z_n^{(3)}(kr) \equiv \mathrm{h}_n^{(1)}(kr) = \left(\frac{\pi}{2kr}\right)^{1/2} \mathrm{H}_{n+1/2}^{(1)}(kr), \tag{3c}$$

$$Z_n^{(4)}(kr) \equiv \mathrm{h}_n^{(2)}(kr) = \left(\frac{\pi}{2kr}\right)^{1/2} \mathrm{H}_{n+1/2}^{(2)}(kr), \tag{3d}$$

where $\mathrm{j}_n(kr)$ and $\mathrm{y}_n(kr)$ are the spherical Bessel functions of first kind and second kind, respectively; $\mathrm{h}_n^{(1)}(kr)$ and $\mathrm{h}_n^{(2)}(kr)$ are the spherical Hankel functions; $\mathrm{J}_{n+1/2}(kr)$, $\mathrm{Y}_{n+1/2}(kr)$, $\mathrm{H}_{n+1/2}^{(1)}(kr)$, $\mathrm{H}_{n+1/2}^{(2)}(kr)$ are the Bessel functions of half-integer order. According to the Biot's poro-elastic theory [16], the wave equations for two-phase saturated porous media are

$$N\nabla^2 u + \nabla[(A+N)e + Q\varepsilon] = \frac{\partial^2}{\partial t^2}(\rho_{11}\boldsymbol{u} + \rho_{12}\boldsymbol{U}) + b\frac{\partial}{\partial t}(\boldsymbol{u} - \boldsymbol{U}), \tag{4a}$$

$$\nabla(Qe + R\varepsilon) = \frac{\partial^2}{\partial t^2}(\rho_{12}\boldsymbol{u} + \rho_{22}\boldsymbol{U}) - b\frac{\partial}{\partial t}(\boldsymbol{u} - \boldsymbol{U}), \tag{4b}$$

where $e = \nabla \cdot \boldsymbol{u}$, $\varepsilon = \nabla \cdot \boldsymbol{U}$, $\rho_{11} = (1-n')\rho_s + \rho_a$, $\rho_{22} = n'\rho_f + \rho_a$, $\rho_{12} = -\rho_a$, n' is the porosity of soil, ρ_s is the mass density of solid phase, ρ_f is the mass density of liquid phase, and ρ_a is the mass density of coupled-phase between the solid phase and liquid phase; $\boldsymbol{u}$ and $\boldsymbol{U}$ are the displacement of solid phase and that of liquid phase, respectively; b is the coefficient related to Darcy's coefficient of permeability; A, N, R, Q are Biot's parameters [16].

The constitutive equations for the elastic saturated porous media can be expressed as

$$\sigma_{ij} = 2N\varepsilon_{ij} + (Ae + Q\varepsilon)\delta_{ij}, \tag{5a}$$

$$S = Qe + R\varepsilon, \tag{5b}$$

where σ_{ij} is the stress of the solid skeleton, S is the stress of the pore fluid, and $\varepsilon_{ij} = (u_{i,j+}u_{j,i})/2$ is the strain of the solid skeleton. To solve the governing equation (4), it is convenient to introduce the following Helmholtz decomposition [16]

$$\boldsymbol{u} = \nabla\Phi + \nabla \times \boldsymbol{H}, \tag{6a}$$

$$\boldsymbol{U} = \nabla\Psi + \nabla \times \boldsymbol{G}, \tag{6b}$$

where Φ and $\boldsymbol{H}$ are potentials associated with the solid phase of the saturated porous material and Ψ and $\boldsymbol{G}$ are potentials associated with the pore fluid phase.

For the incident SV wave with an incident angle δ and a frequency ω, its displacement vector in x–z plane can be expressed as

$$\boldsymbol{u}^{\mathrm{i}} = a_0(-\cos\delta\boldsymbol{e}_x + \sin\delta\boldsymbol{e}_z) \times \exp\{\mathrm{i}k_0(x\sin\delta + z\cos\delta) - \mathrm{i}\omega t\}, \tag{7}$$

where the superscript "i" denotes the incidence of the seismic wave; $\boldsymbol{e}_x$ and $\boldsymbol{e}_z$ are the unit vectors in x and z directions, respectively; a_0 is the displacement amplitude of the incident SV wave, and k_0 is the wave number of incident wave. According to wave theory, there exists a critical angle:

$$\delta_{\mathrm{cr}} = \sin^{-1}\left(\frac{h_0}{k_0}\right), \tag{8}$$

where $h_0 = \omega/\alpha_0$, $k_0 = \omega/\beta_0$ denote the wave number of P wave and SV wave in the half-space, respectively; α_0, β_0 are the velocity of P and SV waves, respectively.

The following two cases are considered:

Case (i): $\delta \le \delta_{\mathrm{cr}}$

When the incident angle is not larger than the critical angle, plane P wave and SV wave are reflected by the free surface. The displacement vector of reflected P waves ($\boldsymbol{u}_1^{\mathrm{r}}$) and that of reflected SV waves ($\boldsymbol{u}_2^{\mathrm{r}}$) are expressed as (omitting the time factor $\exp(-\mathrm{i}\omega t)$ in the following expressions):

$$(\mathrm{P}):\ \boldsymbol{u}_1^{\mathrm{r}} = K_1 a_0(\beta_0/\alpha_0)(\boldsymbol{e}_x\sin\gamma - \boldsymbol{e}_z\cos\gamma) \times \exp\{\mathrm{i}h_0(x\sin\gamma - z\cos\gamma)\}, \tag{9a}$$

$$(\mathrm{SV}):\ \boldsymbol{u}_2^{\mathrm{r}} = K_2 a_0(\boldsymbol{e}_x\cos\delta + \boldsymbol{e}_z\sin\delta) \times \exp\{\mathrm{i}k_0(x\sin\delta - z\cos\delta)\}, \tag{9b}$$

where the superscript "r" refers to reflection by free surface of the half-space; γ is the reflection angle of P waves; K_1 and K_2 are the reflection coefficients that can be expressed as

$$K_1 = \frac{-(\alpha_0/\beta_0)^2\sin 4\delta}{\sin 2\gamma\sin 2\delta + (\alpha_0/\beta_0)^2\cos^2 2\delta}, \tag{10a}$$

$$K_2 = \frac{\sin 2\gamma\sin 2\delta - (\alpha_0/\beta_0)^2\cos^2 2\delta}{\sin 2\gamma\sin 2\delta + (\alpha_0/\beta_0)^2\cos^2 2\delta}, \tag{10b}$$

in which $\gamma = \arcsin(\alpha_0/\beta_0\sin\delta)$.

Case(ii): $\delta > \delta_{\mathrm{cr}}$

When the incident angle is larger than the critical angle, for the reflected SV wave $\boldsymbol{u}_2^{\mathrm{r}}$, there is no change in its magnitude of displacement, but there exists a phase change with respect to the incident angle. There is no reflected P wave, the reflection wave $\boldsymbol{u}_1^{\mathrm{r}}$ is a surface wave, which propagates along the ground surface and attenuates according to the distance to the free surface, and can be expressed as

$$\boldsymbol{u}_1^{\mathrm{r}} = a_0(\beta_0/\alpha_0)S(\boldsymbol{e}_x\sin\delta - \mathrm{i}\nu\boldsymbol{e}_z) \times \exp(k_0\nu z) \times \exp\{\mathrm{i}(-\xi + k_0 x\sin\delta)\}, \tag{11a}$$

$$\boldsymbol{u}_2^{\mathrm{r}} = a_0(\boldsymbol{e}_x\cos\delta + \boldsymbol{e}_z\sin\delta) \times \exp(-2\mathrm{i}\xi) \times \exp\{\mathrm{i}k_0(x\sin\delta - z\cos\delta)\}, \tag{11b}$$

where

$$S = \frac{-\sin 4\delta}{\left(\cos^4 2\delta + 4\nu^2 \sin^2 2\delta \sin^2 \delta\right)^{1/2}}, \tag{12a}$$

$$\nu = \frac{\left(\alpha_0^2/\beta_0^2 \sin^2 \delta - 1\right)^{1/2}}{\alpha_0/\beta_0}, \tag{12b}$$

$$\tan \xi = \frac{2\nu \sin 2\delta \sin \delta}{\cos^2 2\delta}. \tag{12c}$$

Then, the resultant total displacement can be expressed as

$$\boldsymbol{u}^{\mathrm{i+r}} = \boldsymbol{u}^{\mathrm{i}} + \boldsymbol{u}_1^{\mathrm{r}} + \boldsymbol{u}_2^{\mathrm{r}}. \tag{13}$$

The above solutions must satisfy the stress-free boundary conditions, i.e.,

$$\boldsymbol{\sigma}_{zz}^{\mathrm{i+r}} = \boldsymbol{\sigma}_{zx}^{\mathrm{i+r}} = \boldsymbol{\sigma}_{zy}^{\mathrm{i+r}} = 0, \quad \text{at } z = 0. \tag{14}$$

2.2 Fourier–Bessel approximation

On the basis of the theory for elastic waves, it is convenient to employ wave potentials to get the displacement solutions. $\boldsymbol{u}^i$ can be derived from $\Psi^{(\mathrm{i})}$ and $\chi^{(\mathrm{i})}$, $\boldsymbol{u}_1^r$ from $\Psi^{(\mathrm{i})}$ and $\Psi^{(\mathrm{r})}$ and $\boldsymbol{u}_2^r$ from $\Psi^{(\mathrm{r})}$ and $\chi^{(\mathrm{r})}$. These potentials have the following spherical wave expansions:

$$\Phi^{(\mathrm{i})} = 0 \quad (A_{mn}^{(\mathrm{i})} = 0), \tag{15a}$$

$$\Psi^{(\mathrm{i})} = \sum_{m,\,n} k_0 B_{mn}^{(\mathrm{i})} Z_n^{(1)}(k_0 r) P_n^m(\mu) \sin m\phi, \tag{15b}$$

$$\chi^{(\mathrm{i})} = \sum_{m,\,n} C_{mn}^{(\mathrm{i})} Z_n^{(1)}(k_0 r) P_n^m(\mu) \cos m\phi, \tag{15c}$$

$$\Phi^{(\mathrm{r})} = \sum_{m,\,n} A_{mn}^{(\mathrm{r})} Z_n^{(1)}(h_0 r) P_n^m(\mu) \cos m\phi, \tag{15d}$$

$$\Psi^{(\mathrm{r})} = \sum_{m,\,n} k_0 B_{mn}^{(\mathrm{r})} Z_n^{(1)}(k_0 r) P_n^m(\mu) \sin m\phi, \tag{15e}$$

$$\chi^{(\mathrm{r})} = \sum_{m,\,n} C_{mn}^{(\mathrm{r})} Z_n^{(1)}(k_0 r) P_n^m(\mu) \cos m\phi, \tag{15f}$$

where the summation is for $m, n = 0, 1, 2, \ldots$, and $m \le n$. The expansion coefficients $\left\{B_{mn}^{(\mathrm{i})}, C_{mn}^{(\mathrm{i})}, A_{mn}^{(\mathrm{r})}, B_{mn}^{(\mathrm{r})}, C_{mn}^{(\mathrm{r})},\right\}$ can be calculated according to Lee [11,12]. The above potentials satisfy their associated scalar wave equations:

$$\nabla^2 \begin{Bmatrix} \Phi \\ \Psi \\ \chi \end{Bmatrix} + \begin{Bmatrix} h_0^2 \Phi \\ k_0^2 \Psi \\ k_0^2 \chi \end{Bmatrix} = 0. \tag{16}$$

In the presence of the alluvial valley, both longitudinal and transverse outgoing spherical waves are reflected back into half-space and the standing waves are refracted into the valley. The reflected waves can be represented by the potentials as

$$\Phi^{(\mathrm{S})} = \sum_{m,\,n} A_{mn}^{(\mathrm{S})} Z_n^{(3)}(h_0 r) P_n^m(\mu) \cos m\phi, \tag{17a}$$

$$\Psi^{(\mathrm{S})} = \sum_{m,\,n} k_0 B_{mn}^{(\mathrm{S})} Z_n^{(3)}(k_0 r) P_n^m(\mu) \sin m\phi, \tag{17b}$$

$$\chi^{(\mathrm{S})} = \sum_{m,\,n} C_{mn}^{(\mathrm{S})} Z_n^{(3)}(k_0 r) P_n^m(\mu) \cos m\phi, \tag{17c}$$

where the superscript "S" denotes reflection by spherical boundary surface in half-space; the spherical Hankel function $Z_n^{(3)}(=\mathrm{h}_n^{(1)})$ is used because the product $\mathrm{h}_n^{(1)}(\,)\exp(-\mathrm{i}\omega t)$ represents an outward travelling wave.

According to Biot's dynamic theory for saturated porous media [16], there are one rotational wave (S) and two dilatational waves known as the first ($\mathrm{P_I}$) and second kind ($\mathrm{P_{II}}$) waves in the saturated porous elastic medium. The potentials of the refracted standing wave can be expressed as:

$$\Phi_1^{(\mathrm{f})} = \sum_{m,\,n} A_{mn}^{(\mathrm{f})} Z_n^{(1)}(h_1 r) P_n^m(\mu) \cos m\phi, \tag{18a}$$

$$\Phi_2^{(\mathrm{f})} = \sum_{m,\,n} B_{mn}^{(\mathrm{f})} Z_n^{(1)}(h_2 r) P_n^m(\mu) \cos m\phi, \tag{18b}$$

$$\Psi^{(\mathrm{f})} = \sum_{m,\,n} k_1 C_{mn}^{(\mathrm{f})} Z_n^{(1)}(k_1 r) P_n^m(\mu) \sin m\phi, \tag{18c}$$

$$\chi^{(\mathrm{f})} = \sum_{m,\,n} D_{mn}^{(\mathrm{f})} Z_n^{(1)}(k_1 r) P_n^m(\mu) \cos m\phi, \tag{18d}$$

where the superscript "f" denotes refraction by spherical boundary surface; h_1, h_2, k_1 are the wave numbers of $\mathrm{P_I}$ wave, $\mathrm{P_{II}}$ wave and SV wave in the spherical alluvial valley, respectively. $\left\{\Phi^{(\mathrm{S})}, \Psi^{(\mathrm{S})}, \chi^{(\mathrm{S})}\right\}$ and $\left\{\Phi_1^{(\mathrm{f})}, \Phi_2^{(\mathrm{f})}, \Psi^{(\mathrm{f})}, \chi^{(\mathrm{f})}\right\}$ satisfy the wave equation (16). $\left\{A_{mn}^{(\mathrm{S})}, B_{mn}^{(\mathrm{S})}, C_{mn}^{(\mathrm{S})}\right\}$, $\left\{A_{mn}^{(\mathrm{f})}, B_{mn}^{(\mathrm{f})}, C_{mn}^{(\mathrm{f})}, D_{mn}^{(\mathrm{f})}\right\}$ are the expansion coefficients and can be determined according to the following boundary conditions:

(1) Continuity of displacement and stress on the border of the spherical alluvial valley ($r = a$)

$$\boldsymbol{u}^{\mathrm{i}} + \boldsymbol{u}^{\mathrm{r}} + \boldsymbol{u}^{\mathrm{s}} = \boldsymbol{u}^{\mathrm{f}}, \tag{19a}$$

$$\boldsymbol{\sigma}^{\mathrm{i}} + \boldsymbol{\sigma}^{\mathrm{r}} + \boldsymbol{\sigma}^{\mathrm{s}} = \boldsymbol{\sigma}^{\mathrm{f}}. \tag{19b}$$

(2) No seepage at the impervious boundary of the valley, i.e.,

$$u_{\mathrm{s,r}}^{\mathrm{f}} - u_{\mathrm{l,r}}^{\mathrm{f}} = 0, \tag{19c}$$

where the subscript "s" denotes the solid phase of the porous valley, "l" denotes the liquid phase, and "r" represents the radial direction.

If the free surface ($z = 0$) and the spherical alluvial valley ($r \le a$; $z \le 0$) are considered simultaneously, the scattered and diffracted waves will exist between the

free surface and the alluvial valley, and a standing wave will then be formed, which can be expressed as:

In half-space:

$$\Phi^{(\mathrm{R})} = \sum_{j,\,m,\,n} A_{mn}^{(j)} Z_n^{(j)}(h_0 r) P_n^m(\mu)\cos m\phi, \tag{20a}$$

$$\Psi^{(\mathrm{R})} = \sum_{j,\,m,\,n} k_0 B_{mn}^{(j)} Z_n^{(j)}(k_0 r) P_n^m(\mu)\sin m\phi, \tag{20b}$$

$$\chi^{(\mathrm{R})} = \sum_{j,\,m,\,n} C_{mn}^{(j)} Z_n^{(j)}(k_0 r) P_n^m(\mu)\cos m\phi, \tag{20c}$$

where the superscript "R" denotes the scattering between the free boundary surface and the spherical boundary surface in the half-space; $j = 1,2$; m, $n = 0,1,2,\ldots,$ and $m \le n$; $\Phi^{(\mathrm{R})}, \Psi^{(\mathrm{R})}, \chi^{(\mathrm{R})}$ satisfy the wave equation (16), separately.

In saturated alluvial valley:

$$\Phi_1^{(\mathrm{F})} = \sum_{m,\,n} A_{mn}^{(\mathrm{F})} Z_n^{(1)}(h_1 r) P_n^m(\mu)\cos m\phi, \tag{21a}$$

$$\Phi_2^{(\mathrm{F})} = \sum_{m,\,n} B_{mn}^{(\mathrm{F})} Z_n^{(1)}(h_2 r) P_n^m(\mu)\cos m\phi, \tag{21b}$$

$$\Psi^{(\mathrm{F})} = \sum_{m,\,n} k_1 C_{mn}^{(\mathrm{F})} Z_n^{(1)}(k_1 r) P_n^m(\mu)\sin m\phi, \tag{21c}$$

$$\chi^{(\mathrm{F})} = \sum_{m,\,n} D_{mn}^{(\mathrm{F})} Z_n^{(1)}(k_1 r) P_n^m(\mu)\cos m\phi, \tag{21d}$$

where superscript "F" denotes reflection by the free boundary surface in the saturated porous medium; $\Phi^{(\mathrm{R})}, \Psi^{(\mathrm{R})}, \chi^{(\mathrm{R})}$ satisfy the wave equation (16), separately.

In Eqs. 20 and 21, there are ten series of unknown coefficients, i.e., $\{A_{mn}^{(1)}, B_{mn}^{(1)}, C_{mn}^{(1)}\}$, $\{A_{mn}^{(2)}, B_{mn}^{(2)}, C_{mn}^{(2)}\}$ and $\{A_{mn}^{(\mathrm{F})}, B_{mn}^{(\mathrm{F})}, C_{mn}^{(\mathrm{F})}, D_{mn}^{(\mathrm{F})}\}$, which can be determined according to the boundary conditions given below. Thus, the final potential functions, and the displacement field and the stress field at any point in the whole space of wave field can be further determined as follows:

In half-space:

Potential functions:

$$\Phi^{(0)} = \Phi^{(\mathrm{i})} + \Phi^{(\mathrm{r})} + \Phi^{(\mathrm{S})} + \Phi^{(\mathrm{R})}, \tag{22a}$$

$$\Psi^{(0)} = \Psi^{(\mathrm{i})} + \Psi^{(\mathrm{r})} + \Psi^{(\mathrm{S})} + \Psi^{(\mathrm{R})} \tag{22b}$$

$$\chi^{(0)} = \chi^{(\mathrm{i})} + \chi^{(\mathrm{r})} + \chi^{(\mathrm{S})} + \chi^{(\mathrm{R})}. \tag{22c}$$

Displacement:

$$\boldsymbol{u}^{(0)} = \boldsymbol{u}^{\mathrm{i}} + \boldsymbol{u}^{\mathrm{r}} + \boldsymbol{u}^{\mathrm{S}} + \boldsymbol{u}^{\mathrm{R}}. \tag{22d}$$

Stress:

$$\boldsymbol{\sigma}^{(0)} = \boldsymbol{\sigma}^{\mathrm{i}} + \boldsymbol{\sigma}^{\mathrm{r}} + \boldsymbol{\sigma}^{\mathrm{S}} + \boldsymbol{\sigma}^{\mathrm{R}}. \tag{22e}$$

In alluvial valley:

Solid-phase:

Total scalar potential function:

$$\Phi^{(1)} = \Phi_1^{(\mathrm{f})} + \Phi_1^{(\mathrm{F})} + \Phi_2^{(\mathrm{f})} + \Phi_2^{(\mathrm{F})}. \tag{23a}$$

Resultant vector potential functions:

$$\boldsymbol{\Psi}^{(1)} = \boldsymbol{\Psi}^{(\mathrm{f})} + \boldsymbol{\Psi}^{(\mathrm{F})}, \tag{23b}$$

$$\boldsymbol{\chi}^{(1)} = \boldsymbol{\chi}^{(\mathrm{f})} + \boldsymbol{\chi}^{(\mathrm{F})}. \tag{23c}$$

Displacement:

$$\boldsymbol{u}_{\mathrm{s}}^{(1)} = \boldsymbol{u}_{\mathrm{s}}^{\mathrm{f}} + \boldsymbol{u}_{\mathrm{s}}^{\mathrm{F}}. \tag{23d}$$

Stress:

$$\boldsymbol{\sigma}_{\mathrm{s}}^{(1)} = \boldsymbol{\sigma}_{\mathrm{s}}^{\mathrm{f}} + \boldsymbol{\sigma}_{\mathrm{s}}^{\mathrm{F}}. \tag{23e}$$

Liquid-phase:

Total scalar potential function:

$$\Phi'^{(1)} = \eta_1(\Phi_1^{(\mathrm{f})} + \Phi_1^{(\mathrm{F})}) + \eta_2(\Phi_2^{(\mathrm{f})} + \Phi_2^{(\mathrm{F})}). \tag{24a}$$

Resultant vector potential functions:

$$\boldsymbol{\Psi}'^{(1)} = \eta_{\mathrm{III}}(\boldsymbol{\Psi}^{(\mathrm{f})} + \boldsymbol{\Psi}^{(\mathrm{F})}), \tag{24b}$$

$$\boldsymbol{\chi}'^{(1)} = \eta_{\mathrm{III}}(\boldsymbol{\chi}^{(\mathrm{f})} + \boldsymbol{\chi}^{(\mathrm{F})}). \tag{24c}$$

Displacement:

$$\boldsymbol{u}_{\mathrm{l}}^{(1)} = \boldsymbol{u}_{\mathrm{l}}^{\mathrm{f}} + \boldsymbol{u}_{\mathrm{l}}^{\mathrm{F}}. \tag{24d}$$

Stress:

$$\boldsymbol{\sigma}_{\mathrm{l}}^{(1)} = \boldsymbol{\sigma}_{\mathrm{l}}^{\mathrm{f}} + \boldsymbol{\sigma}_{\mathrm{l}}^{\mathrm{F}}. \tag{24e}$$

where η_{I}, η_{II}, η_{III} are the amplitude ratios of potentials for solid and fluid phases of the saturated porous media. The above potential functions can be determined by appropriate boundary conditions:

At the interface between the spherical alluvial valley and the half-space, the displacement and stress are continuous, i.e.,

$$\boldsymbol{u}^{(0)} = \boldsymbol{u}^{(1)}, \quad \boldsymbol{\sigma}^{(0)} = \boldsymbol{\sigma}^{(1)} \quad (r = a). \tag{25a}$$

The interface is assumed as impermeable, i.e., no seepage occurs:

$$\boldsymbol{u}_{\mathrm{s},r}^{(1)\mathrm{f+F}} - \boldsymbol{u}_{\mathrm{l},r}^{(1)\mathrm{f+F}} = 0 \quad (r = a). \tag{25b}$$

Substituting Eqs. (19a)–(19c) into Eqs. (25a)–(25b), we have

$$\boldsymbol{u}^{\mathrm{R}} = \boldsymbol{u}^{\mathrm{F}}, \quad \boldsymbol{\sigma}^{\mathrm{R}} = \boldsymbol{\sigma}_{\mathrm{s}}^{\mathrm{F}} + \boldsymbol{\sigma}_{\mathrm{l}}^{\mathrm{F}}, \quad \boldsymbol{u}_{\mathrm{s},r}^{\mathrm{F}} - \boldsymbol{u}_{\mathrm{l},r}^{\mathrm{F}} = 0 \quad (r = a). \tag{26}$$

On the free surface of half-space (i.e., $z = 0$, $x^2 + y^2 \ge a$):

$$\sigma_{zz}^{(0)} = \sigma_{zx}^{(0)} = \sigma_{zy}^{(0)} = 0, \tag{27a}$$

which is equivalent to the following expression in the spherical coordinates ($r \geq a, 0 \leq \phi \leq 2\pi, \theta = \pi/2$):

$$\sigma_{\theta\theta}^{(0)} = \sigma_{\theta r}^{(0)} = \sigma_{\theta\phi}^{(0)} = 0. \tag{27b}$$

Considering the boundary condition expressed in Eq. (13), Eq. (22e) can be rewritten as

$$\boldsymbol{\sigma}^{\mathrm{S}} + \boldsymbol{\sigma}^{\mathrm{R}} = 0, \tag{27c}$$

while on the free surface of the alluvial valley ($z = 0$, $x^2 + y^2 \leq a$),

$$\sigma_{zz}^{(1)} = \sigma_{zx}^{(1)} = \sigma_{zy}^{(1)} = 0. \tag{27d}$$

In the spherical coordinates, Eq. (27d) is equivalent to ($r \leq a, 0 \leq \phi \leq 2\pi, \theta = \pi/2$)

$$\sigma_{\theta\theta}^{(1)} = \sigma_{\theta r}^{(1)} = \sigma_{\theta\phi}^{(1)} = 0. \tag{27e}$$

For the permeable boundary conditions, we have

$$\sigma_{1,rr}^{(1)} = 0. \tag{27f}$$

In the above boundary value problem, there are ten series of unknowns, i.e., $\{A_{mn}^{(1)}, B_{mn}^{(1)}, C_{mn}^{(1)}; A_{mn}^{(2)}, B_{mn}^{(2)}, C_{mn}^{(2)}; A_{mn}^{(\mathrm{F})}, B_{mn}^{(\mathrm{F})}, C_{mn}^{(\mathrm{F})}, D_{mn}^{(\mathrm{F})}\}$ ($n = 0, 1, 2$), which can be determined by using Fourier–Bessel series expansion technique. Symbolically, for each m, a system of equations can be established as

$$\sum_{j=0}^{\infty} \ell_{ij} x_j = n_i, \quad i = 0, 1, 2, \ldots, \tag{28}$$

where ℓ_{ij} is known coefficients of an infinite matrix, x_i is the unknown infinite sequence, and n_i is a known infinite sequence. Both the coefficients ℓ_{ij} and the sequence n_i can be evaluated numerically. A standard way to solve for the unknown x_i is to truncate the matrix into a finite size array and then invert the finite matrix. This procedure gives well convergent results when the matrix is essentially banded with terms close to the diagonal being much large in magnitude as compared with the off-diagonal terms [12].

2.3 Determination of surface displacements

The predictions of the displacement amplitudes at various points along the surface of the saturated alluvial valley and the surface of the half-space near the hemispherical valley are important from the earthquake engineering point of view. Once the unknown wave potentials are obtained, the surface displacements in the half-space can be determined as

$$u_r = \frac{1}{r} \sum_{j,\,m,\,n} \left[A_{mn}^{(j)} d_{s11}^{(k)} + B_{mn}^{(j)} d_{s12}^{(k)} + C_{mn}^{(j)} d_{s13}^{(k)} \right] \times P_n^m(\mu) \cos m\phi, \tag{29a}$$

$$u_\theta = \frac{1}{r} \sum_{j,\,m,\,n} \left[\left(A_{mn}^{(j)} d_{s21}^{(k)} + C_{mn}^{(j)} d_{s23}^{(k)} \right) \frac{\mathrm{d}P_n^m(\mu)}{\mathrm{d}\theta} + k_0 B_{mn}^{(j)} d_{s22}^{(k)} \frac{mr}{\sin\theta} P_n^m(\mu) \right] \cos m\phi, \tag{29b}$$

$$u_\phi = \frac{1}{r} \sum_{j,\,m,\,n} \left[\frac{-m}{\sin\theta} \left(A_{mn}^{(j)} d_{s21}^{(k)} + C_{mn}^{(j)} d_{s23}^{(k)} \right) P_m^n(\mu) \frac{\mathrm{d}P_n^m(\mu)}{\mathrm{d}\theta} + r(n+m) k_0 B_{mn}^{(j)} d_{s23}^{(k)} \frac{\mathrm{d}P_n^m(\mu)}{\mathrm{d}\theta} \right] \sin m\phi. \tag{29c}$$

Similarly, the displacements for the alluvial valley are expressed as:

$$u_r = \frac{1}{r} \sum_{j,\,m,\,n} \left[A_{mn}^{(j)} d_{v11}^{(k)} + B_{mn}^{(j)} d_{v12}^{(k)} + C_{mn}^{(j)} d_{v13}^{(k)} + D_{mn}^{(j)} d_{v14}^{(k)} \right] P_n^m(\mu) \cos m\phi, \tag{30a}$$

$$u_\theta = \frac{1}{r} \sum_{j,\,m,\,n} \left[\left(A_{mn}^{(j)} d_{v21}^{(k)} + B_{mn}^{(j)} d_{v22}^{(k)} + D_{mn}^{(j)} d_{v24}^{(k)} \right) \frac{\mathrm{d}P_n^m(\mu)}{\mathrm{d}\theta} + k_1 C_{mn}^{(j)} d_{v23}^{(k)} \frac{mr}{\sin\theta} P_n^m(\mu) \right] \cos m\phi, \tag{30b}$$

$$u_\phi = \frac{1}{r} \sum_{j,\,m,\,n} \left[\frac{-m}{\sin\theta} \left(A_{mn}^{(j)} d_{v21}^{(k)} + B_{mn}^{(j)} d_{v22}^{(k)} + D_{mn}^{(j)} d_{v24}^{(k)} \right) P_m^n(\mu) \frac{\mathrm{d}P_n^m(\mu)}{\mathrm{d}\theta} + r(n+m) k_1 C_{mn}^{(j)} d_{v23}^{(k)} \frac{\mathrm{d}P_n^m(\mu)}{\mathrm{d}\theta} \right] \sin m\phi, \tag{30c}$$

where $d_{s11}^{(k)} = nZ_n^{(k)}(h_0 r) - h_0 r Z_{n+1}^{(k)}(h_0 r)$, $d_{s12}^{(k)} = 0$, $d_{s13}^{(k)} = n(n+1)Z_n^{(k)}(k_0 r)$, $d_{s21}^{(k)} = Z_n^{(k)}(h_0 r)$, $d_{s22}^{(k)} = Z_n^{(k)}(k_0 r)$, $d_{s23}^{(k)} = (n+1)Z_n^{(k)}(k_0 r) - k_0 r Z_{n+1}^{(k)}(k_0 r)$; $d_{v11}^{(k)} = nZ_n^{(k)}(h_1 r) - h_1 r Z_{n+1}^{(k)}(h_1 r)$, $d_{v12}^{(k)} = nZ_n^{(k)}(h_2 r) - h_2 r Z_{n+1}^{(k)}(h_2 r)$, $d_{v13}^{(k)} = 0$, $d_{v14}^{(k)} = n(n+1)Z_n^{(k)}(k_1 r)$, $d_{v21}^{(k)} = Z_n^{(k)}(h_1 r)$, $d_{v22}^{(k)} = Z_n^{(k)}(h_2 r)$, $d_{v23}^{(k)} = Z_n^{(k)}(k_1 r)$, $d_{v24}^{(k)} = (n+1)Z_n^{(k)}(k_1 r) - k_1 r Z_{n+1}^{(k)}(k_1 r)$; $m, n = 0, 1, 2, \ldots,$ and $m \leq n$; $j =$ i, r, 1, 2, S, f, F; if $j =$ i, r, 1, f, then $k = 1$; if $j = 2$, then $k = 2$; if $j = S$, then $k = 3$; $k = 1, 2, 3$ represent the three kinds of spherical Bessel functions. Equation (30) can be transformed into the rectangular coordinate as

$$\begin{Bmatrix} u_x \\ u_y \\ u_z \end{Bmatrix} = \begin{bmatrix} \sin\theta\cos\phi & \cos\theta\cos\phi & -\sin\phi \\ \sin\theta\sin\phi & \cos\theta\sin\phi & \cos\phi \\ \cos\theta & -\sin\theta & 0 \end{bmatrix} \begin{Bmatrix} u_r \\ u_\theta \\ u_\phi \end{Bmatrix}. \tag{31}$$

Then, the displacement amplitudes of the solid phase are determined by

$$|u_x| = \left[\mathrm{Re}^2(u_x) + \mathrm{Im}^2(u_x)\right]^{\frac{1}{2}},$$
$$|u_y| = \left[\mathrm{Re}^2(u_y) + \mathrm{Im}^2(u_y)\right]^{\frac{1}{2}},$$
$$|u_z| = \left[\mathrm{Re}^2(u_z) + \mathrm{Im}^2(u_z)\right]^{\frac{1}{2}},$$

where $\mathrm{Re}(\cdot)$ and $\mathrm{Im}(\cdot)$ represent the real and the imaginary parts of the complex argument, respectively.

3 Results and discussions

In this section, a comparison is made between the present model and the previous single-phase model for simulating the surface displacement response of a hemispherical valley. Furthermore, a parametric study is conducted to examine the influences of wavelength and angle of incidence on the surface displacement amplitudes.

For convenience, the following dimensionless frequency η is introduced:

$$\eta = k_0 a/\pi = 2a/\lambda_0, \tag{32}$$

where λ_0 is the wavelength of the incident SV wave. The magnification coefficient of displacement is defined as

$$U_x = u_x/a_0, \quad U_y = u_y/a_0, \quad U_z = u_z/a_0. \tag{33}$$

The properties of the media are shown in Table 1.

Table 1 Properties of materials

Saturated hemispherical alluvial valley	
A/Pa	44.5×10^8
N/Pa	27.6×10^8
R/Pa	32.6×10^7
Q/Pa	74.3×10^7
n'	0.660
$\rho_s/(\mathrm{kg\ m^{-3}})$	2.6×10^3
$\rho_f/(\mathrm{kg\ m^{-3}})$	1.0×10^3
Elastic half-space	
λ/Pa	22.4×10^9
μ/Pa	29.9×10^9
$\rho/(\mathrm{kg\ m^{-3}})$	2.65×10^3

3.1 Comparison between the single-phase and two-phase models

A comparison between the previous single-phase model [12] and the present two-phase model is shown in Figs. 3 and 4. Note that in Figs. 3, 4, 5, 6, 7, 8 and 9, "loop" symbols denote the original surface edge between the hemispherical alluvial valley and the half-space, i.e., ($r = a$, $z = 0$), and solid lines denote the displacements of the above edge induced by SV waves.

Two different normalized wave frequencies (i.e., $\eta = 0.5$ and $\eta = 1.0$) with different incident wave angles (i.e., $\delta = 30°$ and $\delta = 60°$) are considered. As shown in Figs. 3 and 4, a significant difference in the magnification coefficient of displacement is observed between the two models; the difference between the two models becomes more obvious with the increase of the incident angle. It is found that, the amplifications of the surface displacements of the valley ($-1 < (x/a) < 1$) by the hemispherical alluvial valley simulated by Biot's dynamic theory are larger than those simulated by one-phase elastic theory.

3.2 Effects of incident wave angle

The incident wave angle is another factor influencing the magnitudes of SV wave-induced displacements. The effects of the incident wave angle on the normalized displacements are demonstrated in Figs. 5 and 6. As shown in the figures, the influence of the incident wave angle on the normalized displacement (U_z) is less for a low wave frequency (e.g. $\eta = 0.5$) than that for a high wave frequency (e.g. $\eta = 1.0$).

Considering the property of materials shown in Table 1, we can obtain the critical incident angle $\delta_{\mathrm{cr}} = \sin^{-1}(h_0/k_0) = 37.1°$ for the plane SV-waves. When $\delta = 0°, 30°$, the incident angle is below the critical angle and the plane waves are reflected. On the other hand, when $\delta = 60°$ the incident angle is beyond the critical angle and uneven surface waves are reflected and are attenuated quickly in the vertical direction. It can be seen from the figures, because of the presence of the hemispherical saturated alluvial valley, the whole displacement field becomes more complicated.

The magnification coefficients of displacements are affected by the wave scattering, this effect is more distinct in the vicinity of the incidental point. Additionally, the maximum magnitude of displacement increases with the increase of the incidental angle. When the incident angle is greater than the critical angle, e.g. $\delta = 60°$, there is a noticeable increase in the magnitude of displacement on the free surface. However, the displacement distribution becomes more complicated when the incidental angles become larger than the critical incident angle. Figures 7 and 8 illustrate the normalized displacement amplitudes in x, y and z directions with different incident wave angles. Figures 7 and 8 give the x-component amplitudes of surface displacements at dimensionless point (x/a, y/a) near the valley for incident plane SV waves. When the incident angle is smaller than the critical angle, the x-component normalized displacement

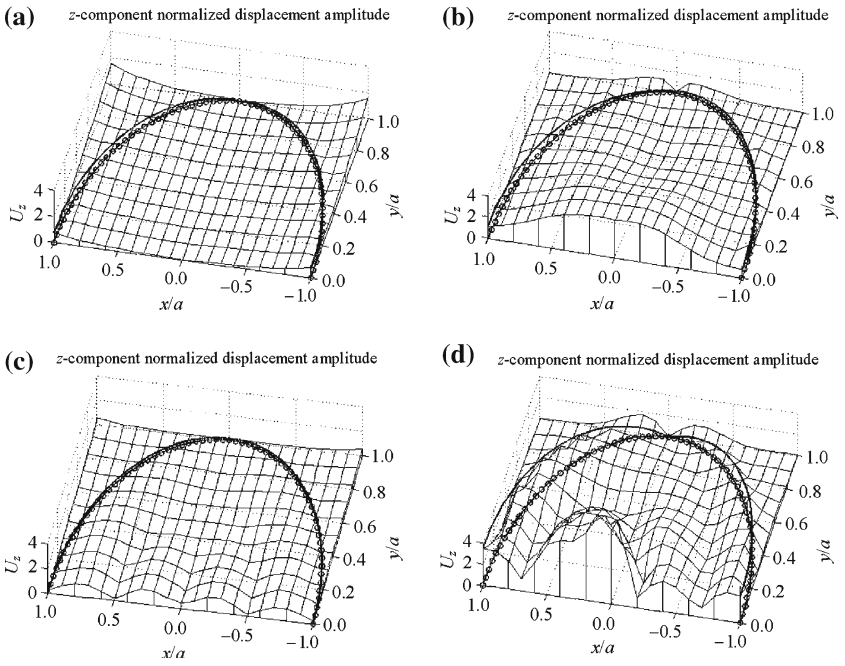

Fig. 3 Comparison of normalized displacement amplitude in z direction (U_z) between single-phase and two-phase models with incident angle $\delta = 30°$: **a** $\eta = 0.5$ (single-phase model), **b** $\eta = 0.5$ (two-phase model), **c** $\eta = 1.0$ (single-phase model), and **d** $\eta = 1.0$ (two-phase model). ($n' = 0.66$)

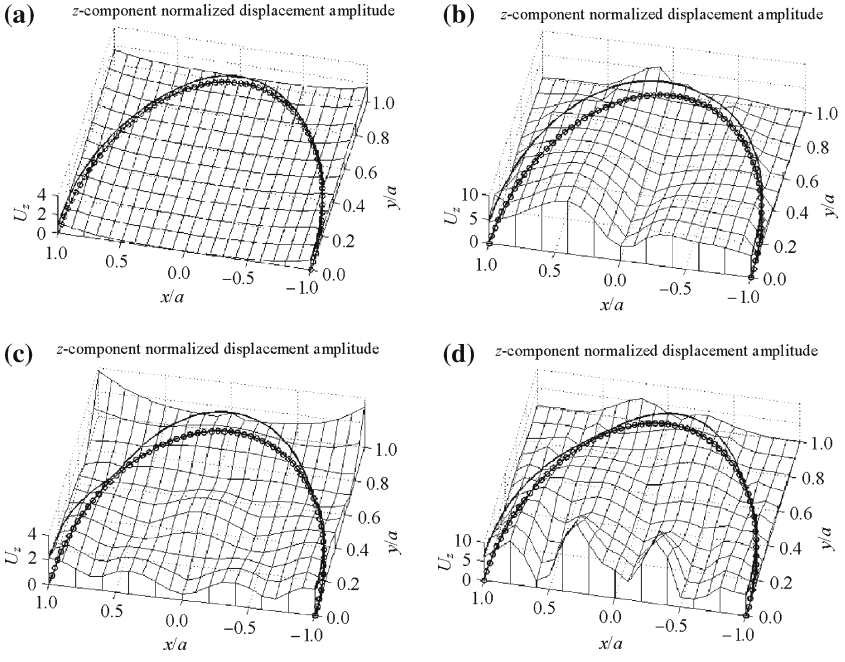

Fig. 4 Comparison of normalized displacement amplitude in z direction (U_z) between single-phase and two-phase models with incident angle $\delta = 60°$: **a** $\eta = 0.5$ (single-phase model), **b** $\eta = 0.5$ (two-phase model), **c** $\eta = 1.0$ (single-phase model), and **d** $\eta = 1.0$ (two-phase model). ($n' = 0.66$)

amplitude is influenced prominently in the region far away from the incidental point owing to the existence of the alluvial valley and takes a greater value. With the increase of the incident angle, the amplitude of displacement increases remarkably and the maximum value is greater than 10.0. However, when the incident angle is greater than the critical angle, there is no obvious change in the amplitude of displacement.

Figures 7 and 8 also give the y- and z-component amplitudes of displacements at dimensionless point (x/a, y/a) near the valley for incident plane SV waves. It is found that the maximum displacement in y direction keeps a constant of 0 at $y/a = 0$ for various incident angles. As shown in Figs. 7 and 8, the magnitudes of U_y and U_z are comparable with those of U_x in the vicinity of alluvial valley.

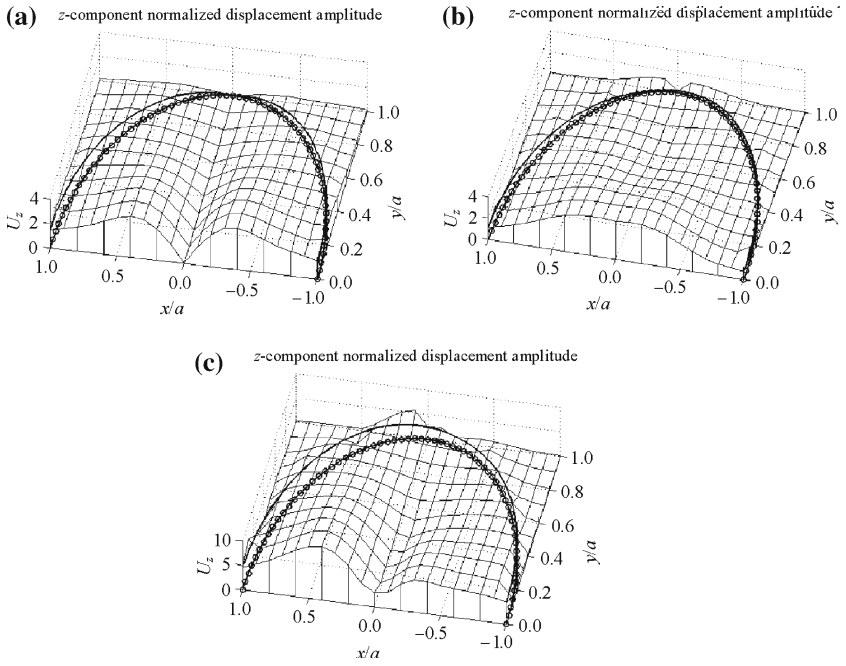

Fig. 5 Effects of incident wave angle on the normalized displacement amplitude in z direction (U_z): **a** $\delta = 0°$, **b** $\delta = 30°$ and **c** $\delta = 60°$ ($\eta = 0.5$ and $n' = 0.66$)

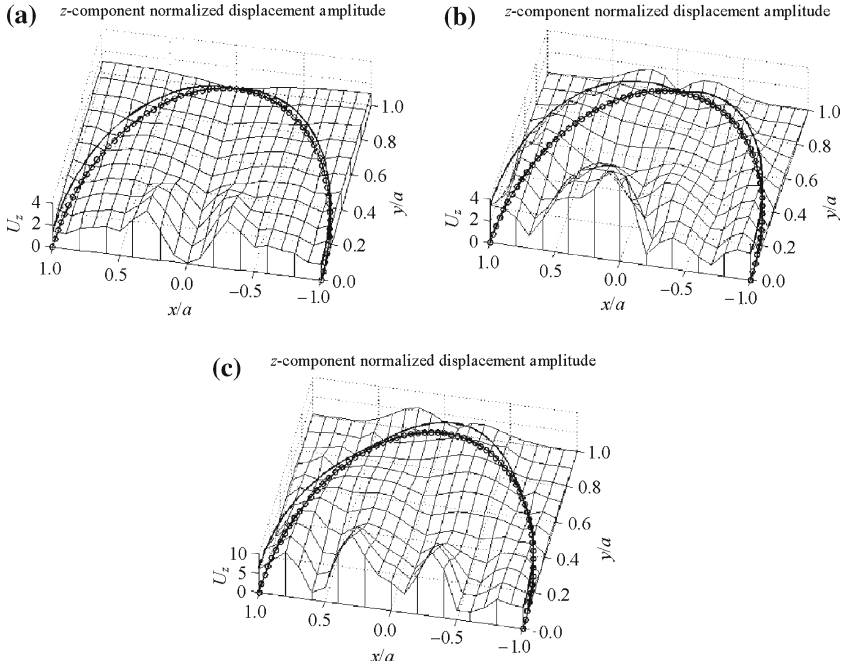

Fig. 6 Effects of incident wave angle on the normalized displacement amplitude in z direction (U_z): **a** $\delta = 0°$, **b** $\delta = 30°$ and **c** $\delta = 60°$ ($\eta = 1.0$ and $n' = 0.66$)

3.3 Effects of wave frequency

The amplitude comparing of normalized displacements in z direction (U_z) between two normalized frequencies i.e., $\eta = 0.5$ and $\eta = 1.0$ (see Figs. 3, 4) indicates that the wave frequency (η) has a great influence on the displacement response of sediments. The distribution of ground surface displacements induced by an SV wave with a high frequency (e.g. $\eta = 1.0$) is more uneven than that with a low frequency (e.g. $\eta = 0.5$) in the examined normalized frequency range.

3.4 Effects of porosity

Porosity of the sediments in the alluvial valley is another influential factor for the earthquake-induced ground motion. Here, we compare the results of two different

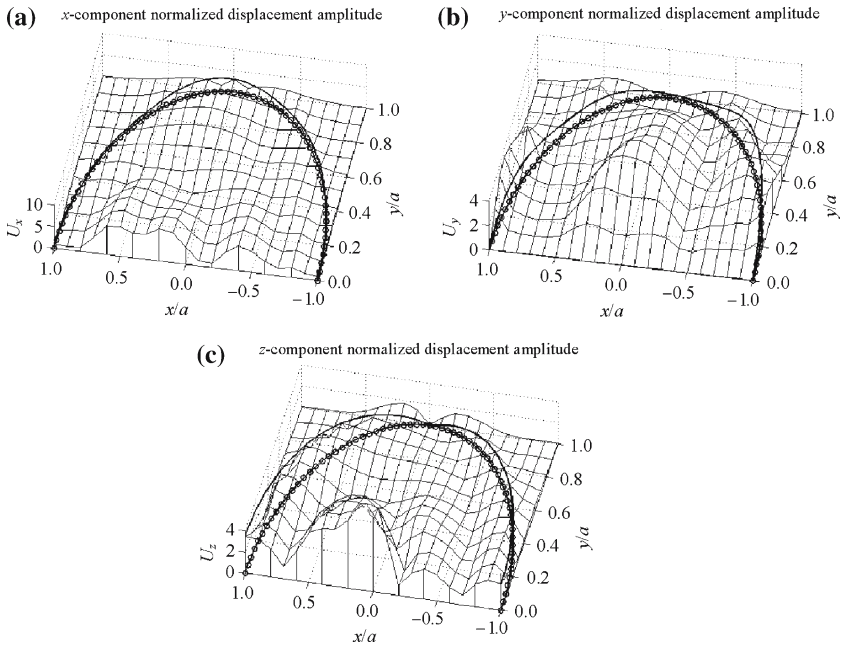

Fig. 7 Distributions of normalized displacements in x, y and z directions at $\delta = 30°$: **a** U_x, **b** U_y and **c** U_z ($\eta = 1.0$ and $n' = 0.66$)

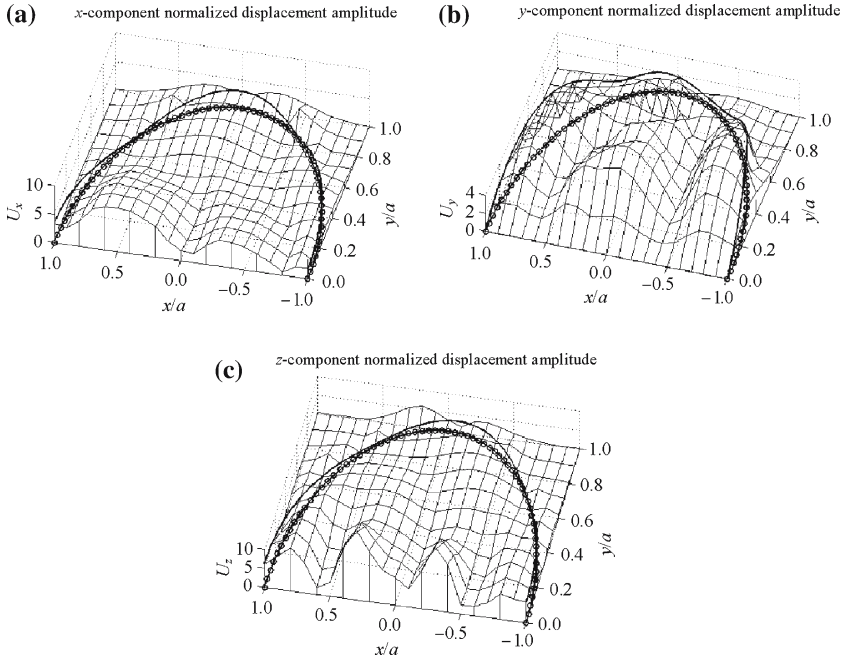

Fig. 8 Distributions of normalized displacements in x, y and z directions at $\delta = 60°$: **a** U_x, **b** U_y and **c** U_z ($\eta = 1.0$ and $n' = 0.66$)

values of porosity ($n' = 0.42$ and $n' = 0.66$), as illustrated in Fig. 9. The figure indicates that the normalized displacement amplitude (U_z) in the sediment with $n' = 0.66$ is greater than that with $n' = 0.42$. This implies that the seismic wave will create a large deformation in the sediments with high porosity. The increase of porosity results in the decrease of the rigidity of the saturated alluvial valley, which in turn increases the level of the aggregation and the magnification of seismic waves in the basin. This shows that it is the thick bathtub soft clay stratification on which the Mexico City is located that enlarges the ground motion and thereby aggravates the damage to the Mexico City during the Mexico earthquake in 1985.

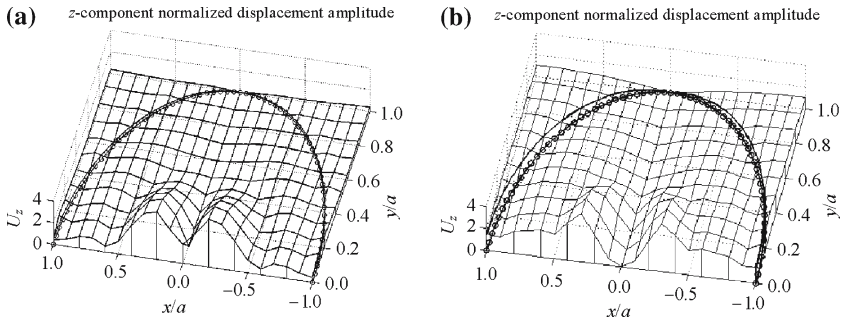

Fig. 9 Distribution of normalized displacements in z-directions (U_z): **a** $n' = 0.42$ and **b** $n' = 0.66$ ($\delta = 0°, \eta = 1.0$)

4 Conclusions

An analytical solution to three-dimensional scattering and diffraction of incident plane SV waves by a hemispherical alluvial valley with saturated soil deposits is obtained by means of *Fourier–Bessel* series expansion technique. The saturated soil deposits are simulated by Biot's dynamic theory for saturated porous media. The displacement response of the soft alluvial valley is further analyzed. The following conclusions based on the numerical results can be drawn:

(1) The amplifications of surface displacements of a hemispherical alluvial valley simulated by Biot's dynamic theory are larger than those simulated by one-phase elastic theory.
(2) The magnification coefficients of displacement on the free surface of the alluvial valley depend mainly on the incident angle, the dimensionless frequency of the incident SV wave. With the increase of the incident angle, the distribution of surface displacement at the hemispherical alluvial valley becomes more complicated.
(3) The porosity of the saturated alluvial valley has great effects on the level of the aggregation and magnification of the ground motion of the alluvial valley. The aggregation and magnification of the ground motion gets more obvious with the increase of the porosity of alluvial valley.

References

1. Anderson, J.G., Bodin, P., Brune, J.N., Prince, J., Singh, S.K., Quaas, R., Onate, M.: Strong ground motion from the Michoacan, Mexico, earthquake. Science **233**(4768), 1043–1049 (1986)
2. Zahardnik, J., Hron, F.: Seismic ground motion of sedimentary valley examples La Molina, Lima Peru. J. Geophys. **62**, 31–37 (1987)
3. Trifunac, M.D.: Scattering of plane SH wave by a semi-cylindrical canyon. Earthq. Eng. Struct. Dyn. **1**, 267–281 (1973)
4. Cao, H., Lee, V.W.: Scattering and diffraction of plane P wave by circular-cylindrical canyons with variable depth-to-width ratio. Soil Dyn. Earthq. Eng. **9**(3), 141–150 (1990)
5. Lee, V.W., Cao, H.: Diffraction of SV wave by circular canyons of various depths. J. Eng. Mech. ASCE **115**(9), 2035–2056 (1989)
6. Todorovska, M., Lee, V.W. Surface motion of shallow circular alluvial valleys for incident plane SH waves: analytical solution. Soil Dyn. Earthq. Eng. **4**, 192–200 (1991)
7. Wong, H.L., Trifunac, M.D.: Surface motion of semi-elliptical alluvial valley for incident plane SH waves. Bull. Seism. Soc. Am. **61**, 1389–1408 (1974)
8. Zhao, C., Valliappan, S.: Seismic wave scattering effects under different canyon topographic and geologic conditions. Soil Dyn. Earthq. Eng. **12**, 129–143 (1993)
9. Fishman, K.L., Ahmad, S.: Seismic response for alluvial valleys subjected to SH, P and SV waves. Soil Dyn. Earthq. Eng. **14**, 249–258 (1995)
10. Lee, V.W.: Displacement near a three-dimensional hemispherical canyon subjected to incident plane wave. Department of Civil Engineering, University of Southern California, Report no. CE 78–16 (1978)
11. Lee, V.W.: A note on the scattering of elastic plane wave by a hemispherical canyon. Soil Dyn. Earthq. Eng. **1**(3), 122–129 (1982)
12. Lee, V.W.: Three-dimensional diffraction of plane P, SV, SH waves by a hemispherical alluvial valley. Soil Dyn. Earthq. Eng. **3**(3), 133–144 (1984)
13. Mow, C.C., Pao, Y.H.: Diffraction of elastic waves and dynamic stress concentration. Rand Report, R-482-PR, New York (1971)
14. Li, W.H., Zhao, C.G.: An analytical solution for the diffraction of plane P-waves by circular cylindrical canyons in a fluid-saturated porous media half space (in Chinese). Chin. J. Geophys. **46**(4), 539–546 (2003)
15. Li, W.H., Zhao, C.G.: Scattering of plane P-waves in alluvial valleys with saturated soil deposits (in Chinese). Chin. J. Geotechn. Eng. **25**(3), 346–351 (2003)
16. Biot, M.A.: Theory of propagation of elastic waves in a fluid-saturated porous soil. J. Acoust. Soc. Am. **28**(2), 168–178 (1956)